View metadata, citation and similar papers at core.ac.uk

brought to you by CORE

provided by MPG.PuRe

Supplementary Information

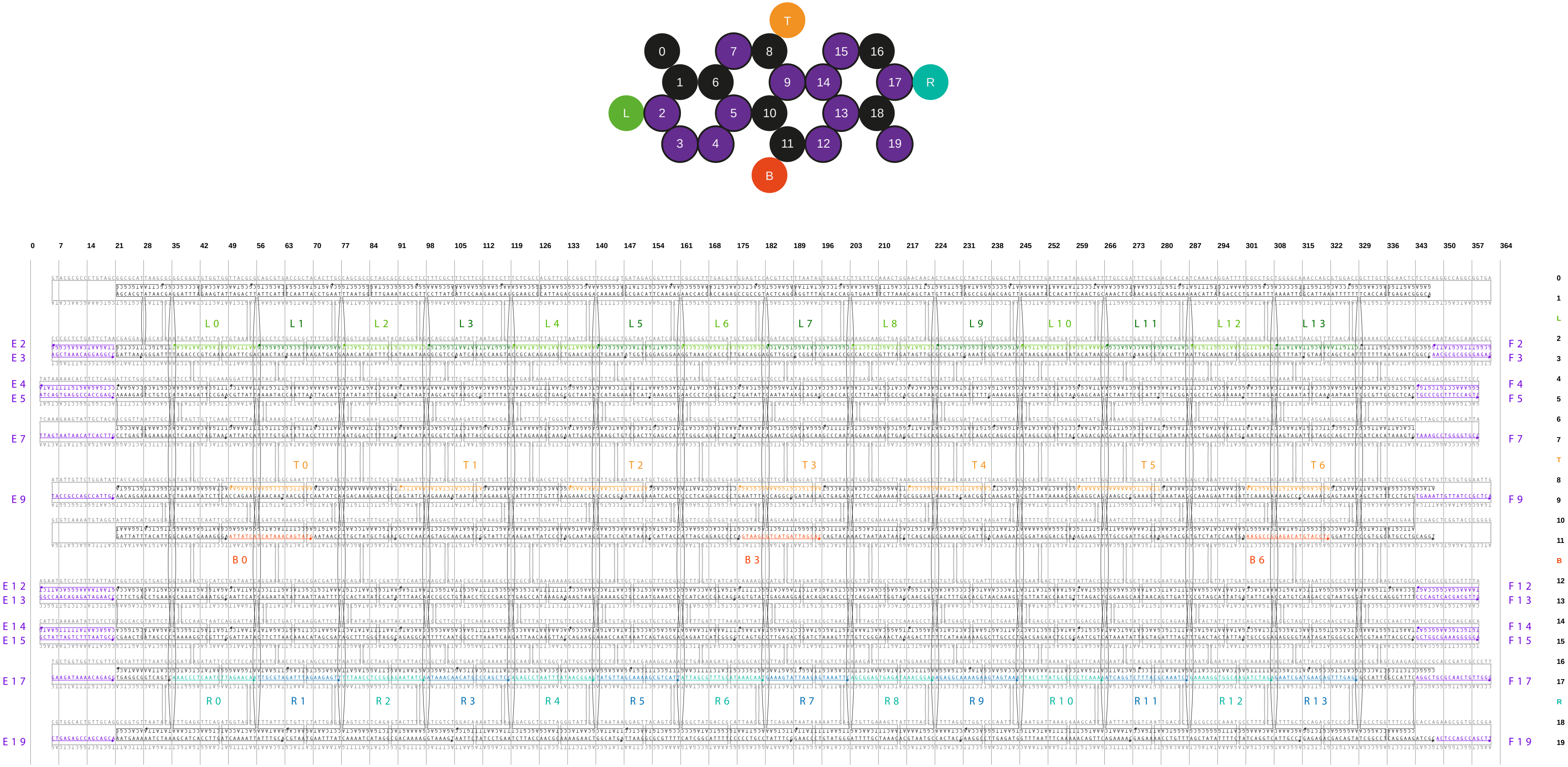

Figure S1 | Cadnano design and oligonucleotide sequences of the various origami L structures.

Top positions T0-T6 are coloured in gold, while bottom positions B0, B3, B6 are coloured in dark orange. Lateral positions L0-L13 and R0-R13 are coloured in green and blue, respectively. Edge positions E2-5, E7, E9, E12-15, E17, E19 and F2-5, F7, F9, F12-15, F17, F19 are coloured in purple. Core staples are coloured in black; M13 p7249 scaffold is coloured in grey. List of functionalized staples can be found in Table S1.

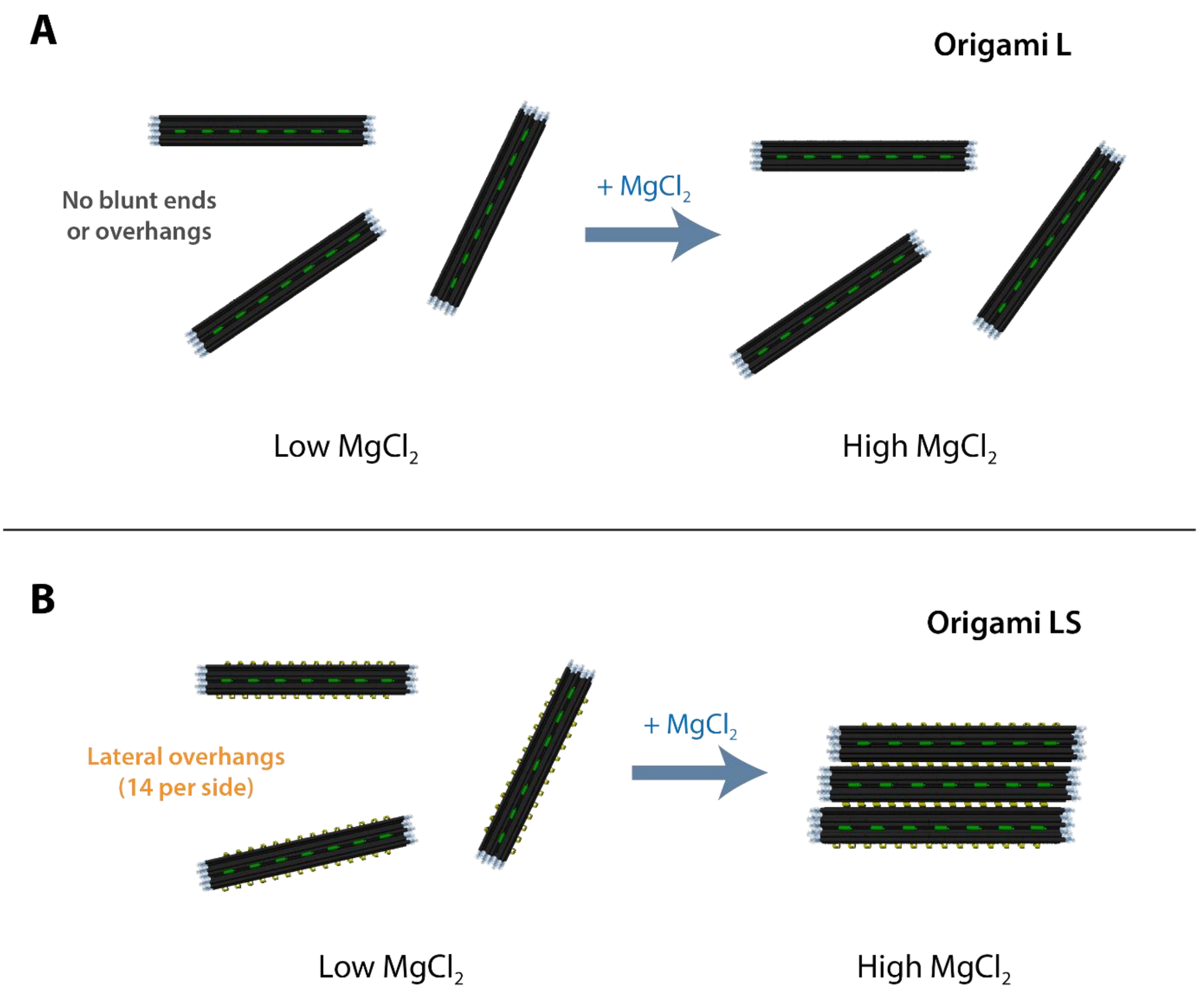

Figure S2 | Depiction of the self-assembly patterns of origami L and LS upon increasing $MgCl_2$. **(A)** Origami L does not possess the ability to polymerize, as it lacks blunt ends or lateral overhangs for establishing intermolecular interactions. **(B)** Origami LS displays 14 lateral self-complementary single-stranded overhangs on both sides, and is therefore able to polymerizes into sheet-like oligomers at high $MgCl_2$ concentrations.

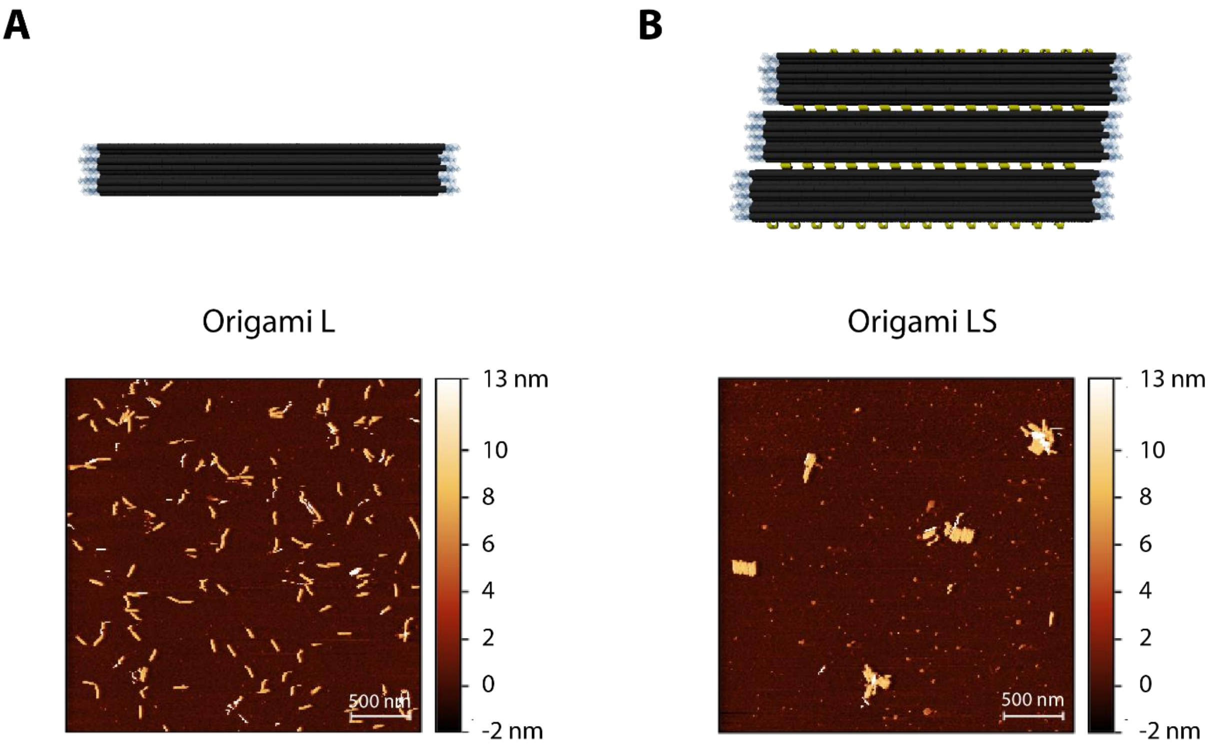

Figure S3 | Self-assembly properties of origami L and origami LS at high $MgCl_2$.

Atomic force microscopy (AFM) images on PLL-mica of origami L lacking blunt ends **(A)** and origami LS displaying 14 lateral self-complementary single-stranded overhangs on both sides **(B)** after incubation with a high $MgCl_2$ buffer (70 mM $MgCl_2$ + 187.5 mM NaCl). As here depicted, whereas origami L **(A)** stays in a monomeric form, origami LS **(B)** polymerizes into sheet-like oligomers.

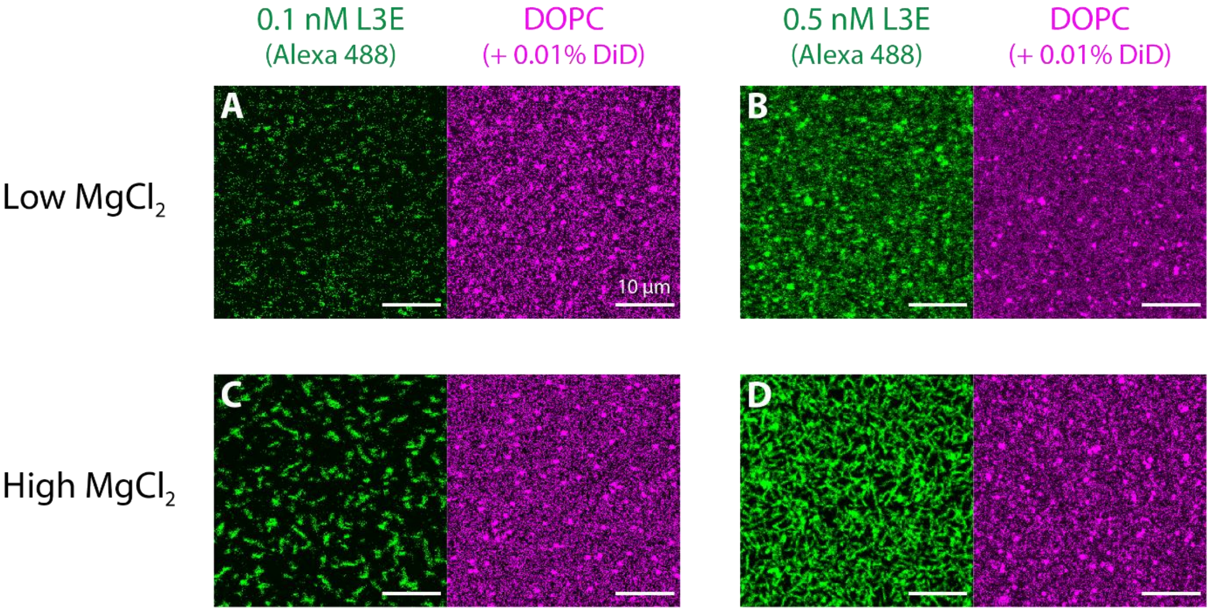

Figure S4 | Binding and polymerization of DNA origami L3E on top of supported lipid bilayers. Zoomed-out images depicting the interaction of 0.1 and 0.5 nM Alexa488-labelled DNA origami L3E displaying 3 TEG-chol anchors (for membrane binding) and blunt ends (for end-to-end self-assembly) with DOPC SLBs (doped with 0.01% DiD). **(A-B)** At low $MgCl_2$ (5 mM $MgCl_2$ + 300 mM NaCl), a mostly homogenous distribution of origami L3E was observed on top of the lipid bilayers. **(C-D)** At high $MgCl_2$ (70 mM $MgCl_2$ + 187.5 mM NaCl) origami filaments were observed on top of the lipid bilayer. While at 0.1 nM, origami L3E formed individual short filaments **(C)**, at 0.5 nM origami L3E self-assembled into a mesh of longer and bundled filaments **(D)**.

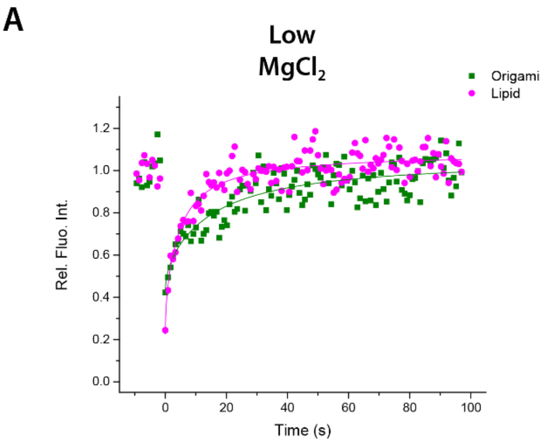

	Origami L3E (Alexa 488)	DOPC SLB (At655-DOPE)
Diffusion ($\mu m^2/s$)	0.194 ± 0.050	0.608 ± 0.096
Mobile fraction	1.109 ± 0.041	1.109 ± 0.050

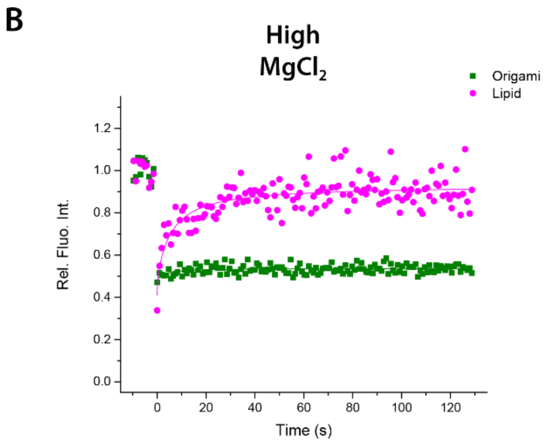

	Origami L3E (Alexa 488)	DOPC SLB (At655-DOPE)
Diffusion ($\mu m^2/s$)	n/a	0.490 ± 0.128
Mobile fraction	0.116 ± 0.017	0.881 ± 0.052

Figure S5 | Fluorescence recovery after photobleaching (FRAP) of membrane-bound origami L3E on DOPC supported lipid bilayers (SLBs).

FRAP data (from Movies S1 and S3), fitted results and calculated diffusion coefficients/mobile fractions of 0.5 nM origami L3E on a DOPC SLB, in the presence of **(A)** low $MgCl_2$ (5 mM $MgCl_2$ + 300 mM NaCl) and **(B)** high $MgCl_2$ (70 mM $MgCl_2$ + 187.5 mM NaCl).

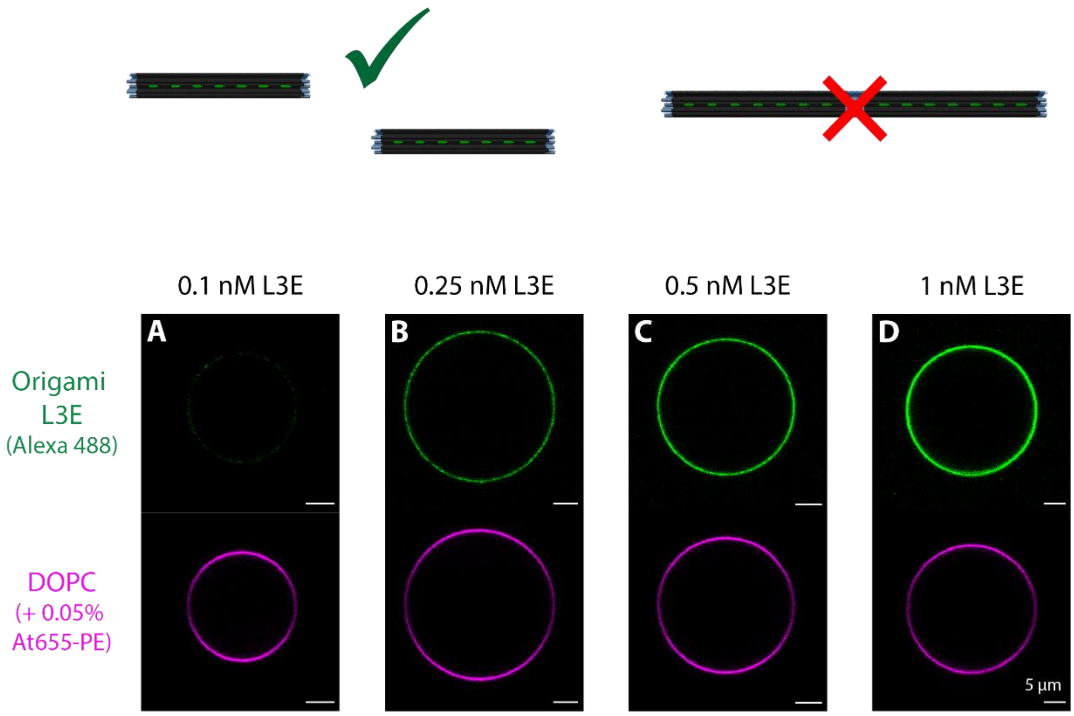

Figure S6 | Interaction of origami L3E with giant unilamellar vesicles at low $MgCl_2$.

Membrane attachment of different bulk concentrations (0.1-1 nM) of Alexa488/TEG-chol-modified origami L3E displaying blunt ends to DOPC GUVs (doped with 0.05% Atto655-DOPE) in the presence of low $MgCl_2$ buffer (5 mM $MgCl_2$ + 300 mM NaCl). Images correspond to equatorial plane slices of GUVs.

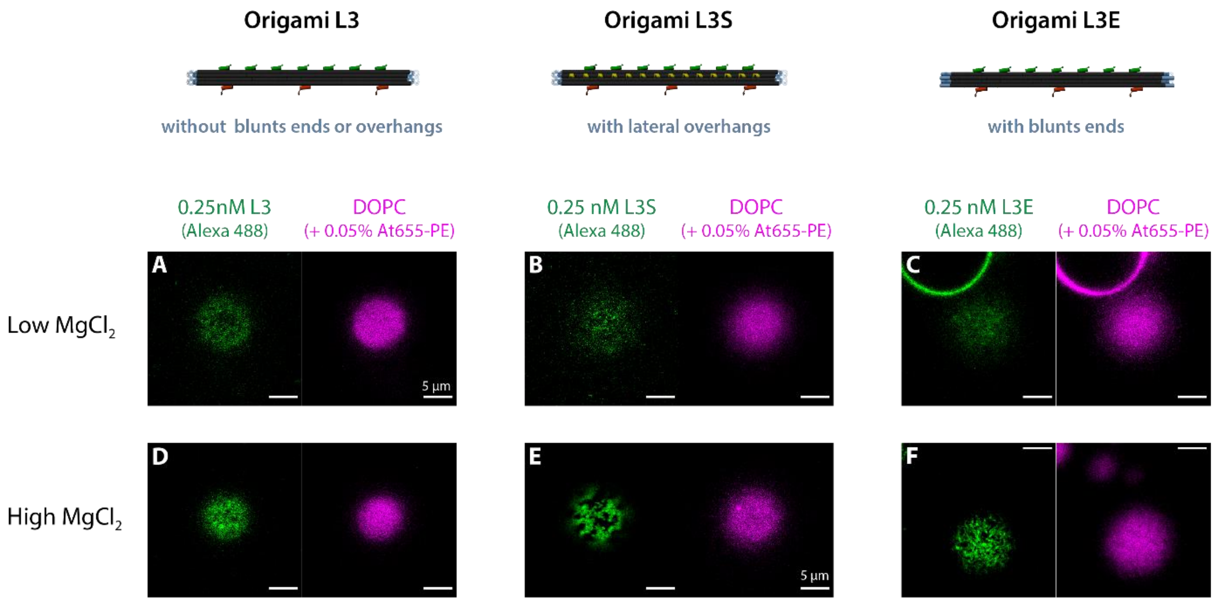

Figure S7 | Triggering self-assembly of membrane-bound origami L3, L3S and L3E.

As depicted for the pole of selected GUVs, at low $MgCl_2$ **(A-C)**, origami L3, L3S and L3E are homogenously distributed on top of DOPC GUVs, corroborating their predominant monomeric state under these conditions. Upon increasing the amount of $MgCl_2$, membrane-bound origami L3 (lacking blunt ends and lateral overhangs) remains homogeneously distributed **(D)**; origami L3S (displayed lateral overhangs) can engage into lateral self-assembly, giving rise to large platforms **(E)**; and finally origami L3E (displaying blunt ends) can polymerize end-to-end, giving rise to a mesh of filaments **(F)**.

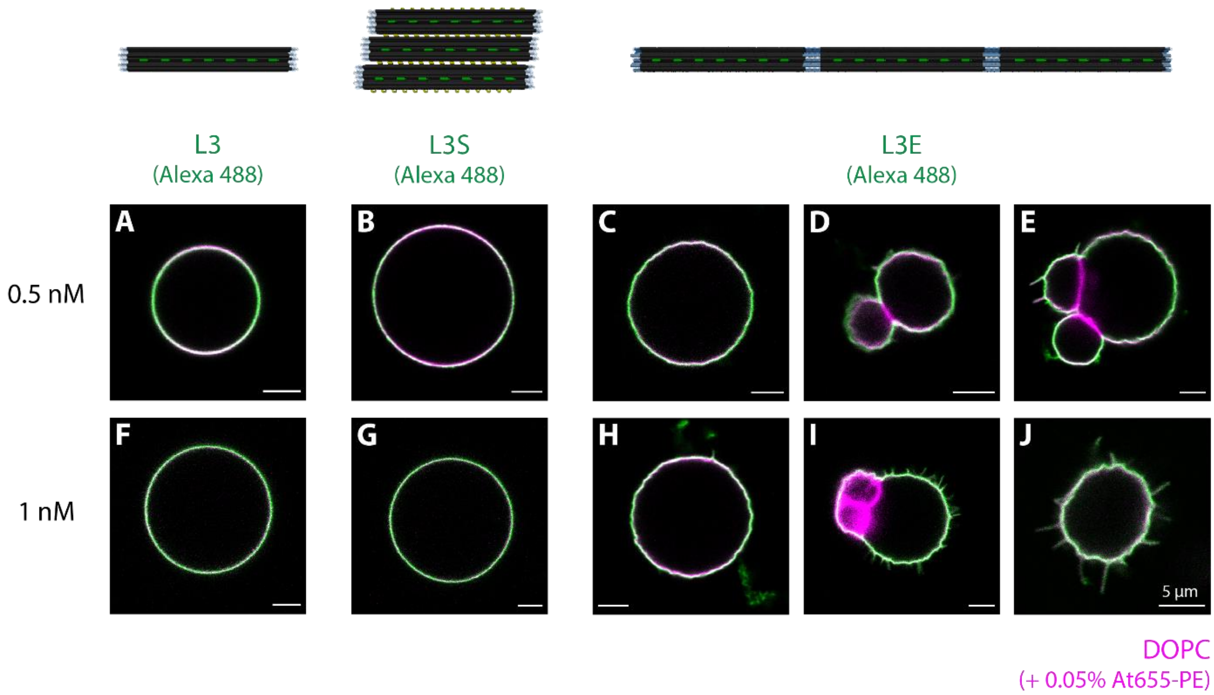

Figure S8 | Membrane deformations by origami L3, L3S and L3E at high $MgCl_2$.

Equatorial plane images of GUVs incubated with 0.5 nM **(A-E)** and 1 nM **(F-J)** origami L3/L3S/L3E at least 90 min prior addition of additional $MgCl_2$. For origami L3 lacking the ability to polymerize **(A, F)** no significant membrane deformations were reported. Similar results were observed for vesicles incubated with origami L3S, able to form lateral origami platform **(B, G)**. On the contrary, for vesicles with membrane-bound origami L3E, extensive remodelling as rough **(C, H)** and spike-like **tubular (D, E, I, J)** deformations were observed, after $MgCl_2$-triggered end-to-end self-assembly of L3E into linear origami aggregates/filaments.

Table S1 | List of functional staples used for various origami L structures.

Oligo	Sequence	Description	Partner staple
TD_00	AAATTCGCCCGGAACAAAGAA**AAAAAACACCAAACCC**	staples with extension for Alexa488 dye	***5'-Alexa488-***
TD_01	ATTCCCATCTATACAAATTCT**AAAAAACACCAAACCC**	***used in all origami***	***GGGTTTGGTGTTTTTT***
TD_02	ATTTATTTCCAATAATAAGA**AAAAAACACCAAACCC**		
TD_03	AAGTGCCGTGGAAAGCGCAGT**AAAAAACACCAAACCC**		
TD_04	CAAGATTTGTTAAAGGCCGCT**AAAAAACACCAAACCC**		
TD_05	TTACTTCAAAAAACCAAAATA**AAAAAACACCAAACCC**		
TD_06	AGACAGGAAATGTGTAGGTAA**AAAAAACACCAAACCC**		
B18_00	ATTATCATCATAAACAGTATG**GCTATGGGTGGTCTGGTT**	staples with extension for TEG-Chol(18)	***5'-Chol-TEG-***
B18_03	GTAAGCGTCATGATTAGCAC**GCTATGGGTGGTCTGGTT**	***used in origami L3, L3E and L3S***	***AACCAGACCACCCATAGC***
B18_06	AAGGCCGGAGACATGTACCTC**GCTATGGGTGGTCTGGTT**		
E_02	TTAGAATCAGAGCGGG	staples for tip-to-tip blunt end interactions	
F_02	GCGGTTTGCGTATTG	***used in origami LE and L3E***	
E_03	AGCTAAACAGGAGGCC		
F_03	AACGCGCGGGGAGAG		
E_04	CCTGAGAAGTGTTTTTATA		
F_04	GGGAAACCTGTCGTGC		
E_05	ATCAGTGAGGCCACCGAGT		
F_05	TGCCCGCTTTCCAGTC		
E_07	TTAGTAATAACATCACTTG		
F_07	TAAAGCCTGGGGTGCC		
E_09	TACCGCCAGCCATTGC		
F_09	TGAAATTGTTATCCGCTCA		
E_12	GTAATAAAAGGGACATTCT		
F_12	TAAAACGACGGCCAGT		
E_13	GGCCAACAGAGATAGAACC		
F_13	CCCAGTCACGACGTTG		
E_14	CAGACAATATTTTTGAATG		
F_14	TGTGCTGCAAGGCGAT		
E_15	GCTATTAGTCTTTAATGCG		
F_15	GCTGGCGAAAGGGGGA		
E_17	GAAGATAAAACAGAGG		
F_17	AGGCTGCGCAACTGTTGGG		
E_19	CTGAGAGCCAGCAGCA		
F_19	ACTCCAGCCAGCTT		
LS_00	**TATATATTT**AATTTACAATAGATAATACAT	staples for lateral oligomerization	
LS_01	**TATATATTT**AAGCAAAAGCGCGCAGAGGCG	***used in origami LS and L3S***	
LS_02	**TATATATTT**CTACCGTGTATCTTCTGACCT		
LS_03	**TATATATTT**ACGGTATTAATAATCGGCTGT		
LS_04	**TATATATTT**AAGAATTAAAATAACATAAAA		
LS_05	**TATATATTT**CCCGATTGATTACCAGCGCCA		
LS_06	**TATATATTT**CCGCCAGCATCAGAGCCGCCA		
LS_07	**TATATATTT**CGGCCACCCATAGGTGTATCA		
LS_08	**TATATATTT**CCTGATACCTCAGCTTGCTTT		
LS_09	**TATATATTT**ATGCGCAGACCGCGACCTGCT		
LS_10	**TATATATTT**AAAATGCAGTCATCAGTTGAG		
LS_11	**TATATATTT**CATTAGAGAGAACCAGACCGG		
LS_12	**TATATATTT**TGACTTTTGAATCGGTTGTAC		
LS_13	**TATATATTT**CTTGTTAAAACGTTAATATTT		
RS_00	**TATATATTT**AAACCCTCAATCTTAGAACAA		
RS_01	**TATATATTT**TTGCGTAGATTTAGAAGAGTT		
RS_02	**TATATATTT**TTTAACCTCCGGAGAATATCA		
RS_03	**TATATATTT**ATAAACAACATGCCCAGCTCC		
RS_04	**TATATATTT**AGAGCCTAATTTATAACGGAG		
RS_05	**TATATATTT**TATGTTAGCAAAAGCGTCATT		
RS_06	**TATATATTT**ATTAGCGTTTGCATAAACAAT		
RS_07	**TATATATTT**GAAAGTATTAAGAGTAAATTC		
RS_08	**TATATATTT**AGCGGAGTGAGATAAACGGAA		
RS_09	**TATATATTT**AGAGGCAAAAGAAGTAGTAAA		
RS_10	**TATATATTT**TTACCTTATGCGCCCTCAAAA		
RS_11	**TATATATTT**ATCAGGTCTTTACGCAAATCT		
RS_12	**TATATATTT**GAAAAGGTGGCAAGATCTAGA		
RS_13	**TATATATTT**GAATCGATGAACAGTTTGAGC		

Table S2 | Fraction of deformed vesicles, upon increasing $MgCl_2$, as a function of total L3E concentration.

[L3E] (nM)	% Deformed vesicles (± st. dev.)	Independent repeats	Total number vesicles (N_{total})
0.1	10.9 ± 10.1%	4	174
0.25	37.1 ± 20.9%	5	316
0.5	65.6 ± 12.1%	5	401
1	70.2 ± 9.6%	4	350

Movie Captions

Movie S1 | FRAP of 0.5 nM origami L3E (Alexa488-labelled, green) on top of DOPC SLB (doped with Atto655-DOPE, magenta), in the presence of a low $MgCl_2$ buffer (5 mM $MgCl_2$ + 300 mM NaCl). Corresponding data represented in Figure 3SA. Scalebar is 5 µm.

Movie S2 | Time-series of $MgCl_2$-triggered polymerization of 0.5 nM origami L3E (Alexa488-labelled, green) on top of DOPC SLB. Addition of $MgCl_2$ happened at timepoint 5:00. Scalebar is 10 µm.

Movie S3 | FRAP of 0.5 nM origami L3E (Alexa488-labelled, green) on top of DOPC SLB (doped with DiD, magenta), in the presence of a high $MgCl_2$ buffer (70 mM $MgCl_2$ + 187.5 mM NaCl). Corresponding data represented in Figure 3SB. Scalebar is 5 µm.

Movies S4 & S5 | Diffusion of 0.1nM origami L3E (Alexa488-labelled, green) on the pole of GUVs (doped with Atto655-DOPE, magenta), after $MgCl_2$-mediated polymerization into membrane-bound end-to-end self-assembled filaments.

Movie S6 | Diffusion of 0.1nM origami L3S (Alexa488-labelled, green) on the pole of GUV (doped with Atto655-DOPE, magenta), after $MgCl_2$-mediated polymerization into membrane-bound laterally self-assembled platforms.

Movie S7 | Characteristic wrinkled membrane deformations on DOPC GUV (doped with Atto655-DOPE, magenta) induced by membrane-bound origami L3E (Alexa488-labelled, green) at 1 nM bulk concentration, after $MgCl_2$-mediated polymerization into filaments. Scalebar is 5 µm.

Movie S8 | Characteristic spike-like tubular deformations on DOPC GUV (doped with Atto655-DOPE, magenta) induced by membrane-bound origami L3E (Alexa488-labelled, green) at 1 nM bulk concentration, after $MgCl_2$-mediated polymerization into filaments. Scalebar is 5 µm.